On the magnetospheric ULF wave counterpart of substorm onset

JGR Space Physics

RESEARCH ARTICLE
10.1029/2019JA027573

On the Magnetospheric ULF Wave Counterpart of Substorm Onset

A. W. Smith[1], I. J. Rae[1], C. Forsyth[1], C. E. J. Watt[2], and K. R. Murphy[3]

[1]Mullard Space Science Laboratory, University College London, Dorking, UK, [2]Department of Meteorology, University of Reading, Reading, UK, [3]Department of Astronomy, University of Maryland, College Park, MD, USA

Key Points:
- Conjugate ionospheric and magnetospheric measurements show exponential growth of ULF waves at rates of ~0.01 s^{-1}
- Magnetospheric ULF wave growth leads the ionosphere by 1–1.5 min, identifying a magnetospheric source
- Large magnetotail ULF power is most commonly observed premidnight (at $X_{GSM} \sim 10R_E$), confirming the conjugate location of auroral beads

Correspondence to:
A. W. Smith,
andy.w.smith@ucl.ac.uk

Citation:
Smith, A. W., Rae, I. J., Forsyth, C., Watt, C. E. J., & Murphy, K. R. (2020). On the magnetospheric ULF wave counterpart of substorm onset. *Journal of Geophysical Research: Space Physics*, *125*, e2019JA027573. https://doi.org/10.1029/2019JA027573

Received 25 OCT 2019
Accepted 6 MAR 2020
Accepted article online 4 APR 2020

Abstract One near-ubiquitous signature of substorms observed on the ground is the azimuthal structuring of the onset auroral arc in the minutes prior to onset. Termed auroral beads, these optical signatures correspond to concurrent exponential increases in ground ultralow frequency (ULF) wave power and are likely the result of a plasma instability in the magnetosphere. Here, we present a case study showing the development of auroral beads from a Time History of Events and Macroscale Interactions during Substorms (THEMIS) all-sky camera with near simultaneous exponential increases in auroral brightness, ionospheric and conjugate magnetotail ULF wave power, evidencing their intrinsic link. We further present a survey of magnetic field fluctuations in the magnetotail around substorm onset. We find remarkably similar superposed epoch analyses of ULF power around substorm onset from space and conjugate ionospheric observations. Examining periods of exponential wave growth, we find the ground- and space-based observations to be consistent, with average growth rates of ~0.01 s^{-1}, lasting for ~4 min. Cross-correlation suggests that the space-based observations lead those on the ground by approximately 1–1.5 min. Meanwhile, spacecraft located premidnight and ~10 R_E downtail are more likely to observe enhanced wave power. These combined observations lead us to conclude that there is a magnetospheric counterpart of auroral beads and exponentially increasing ground ULF wave power. This is likely the result of the linear phase of a magnetospheric instability, active in the magnetotail for several minutes prior to auroral breakup.

1. Introduction

During a magnetospheric substorm, magnetic energy is stored and then explosively released in the magnetotail (Akasofu, 1964; McPherron, 1970). Interaction of Earth's magnetic field with the interplanetary magnetic field (IMF) results in the opening of magnetic flux through the process of magnetic reconnection on the dayside magnetopause. The newly opened magnetic flux is dragged across the polar caps by the ambient solar wind flow and stored in the magnetotail lobes; this process forms the growth phase of a substorm (McPherron, 1970). Later, during the substorm expansion phase, the open magnetospheric flux is rapidly closed through reconnection in the nightside magnetotail (Hones, 1976). In the expansion phase, magnetotail currents are diverted through the ionosphere by a set of field-aligned current systems (McPherron et al., 1973), with the auroral electrojets causing large bays in ground-based magnetometer data (Akasofu & Chapman, 1961; Davis & Sugiura, 1966; Heppner, 1954) and particle precipitation causing bright auroral displays (Akasofu, 1964). The start of the expansion phase (often called substorm onset) is classically defined from ground-based optical observations as the time at which the most equatorward auroral arc brightens and is observed to move poleward (Akasofu, 1964, 1977). Substorm onset is also associated with a large growth in ultralow frequency (ULF) wave power (Rae, Mann, Murphy, et al., 2009; Rae et al., 2012; Rae & Watt, 2016; Voronkov et al., 2003).

In general, there are two main phenomenological models that are invoked to explain substorm onset. In the first, known as the near-Earth neutral line (NENL) model, magnetic reconnection starts in the mid-magnetotail (~20–30 R_E from the Earth, $1R_E = 6{,}371$ km), causing earthward directed flows that subsequently destabilize the plasma sheet closer to the planet (e.g., Baker et al., 1996; Shiokawa et al., 1997). In the second model, a disturbance at the inner edge of the plasma sheet (~10 R_E from the Earth) causes a current disruption (CD), leading to reconnection further from the Earth (e.g., Lui et al., 1991; Roux et al., 1991). These are sometimes known as the "outside-in" or "inside-out" models, respectively. Case studies have often provided example substorms that are best represented by one of the models (e.g., Angelopoulos et al., 2008;

Henderson, 2009; Hwang et al., 2014; Kepko et al., 2009; Liang et al., 2008; Rae, Mann, Angelopoulos, et al., 2009; Rae et al., 2010), or by both (Murphy et al., 2014). A third model of substorm onset has garnered attention in recent years, in which substorms are initiated by an intrusion of plasma from farther down the magnetotail (Nishimura et al., 2010). The precise sequence of events that leads to substorm onset is unclear to this day; the lack of clarity is largely due to a lack of spatial and temporal coverage over the vast three-dimensional region within which the substorm process occurs. Nonetheless, three phenomena are intrinsically related to onset: auroral intensification, geomagnetic bays, and ULF waves (e.g., Rae et al., 2012; Walsh et al., 2010).

Azimuthal structure is often observed for several minutes in what will later become the onset arc (Davis, 1962); such patterns are known as auroral beads (Henderson, 1994) or azimuthally spaced auroral forms (Elphinstone et al., 1995). Analysis of data from all-sky imagers (ASIs) has found that the spatial scales of beads are between ~30 and 150 km in the ionosphere (Chang & Cheng, 2015; Friedrich et al., 2001; Kalmoni et al., 2015, 2017; Motoba et al., 2012; Murphy et al., 2014; Rae, Mann, Angelopoulos, et al., 2009; Rae et al., 2010; Sakaguchi et al., 2009). It has also been shown that these auroral beads are related to the spatially and temporally coincident increases in ground ULF power (Milling et al., 2008; Murphy et al., 2009; Rae, Mann, Angelopoulos, et al., 2009; Rae, Mann, Murphy, et al., 2009; Rae et al., 2011, 2012, 2017; Walsh et al., 2010). Auroral beads are observed in the majority (>90%) of onset arcs (Kalmoni et al., 2017; Nishimura et al., 2016), suggesting that there is a consistent phenomenon related to the auroral onset arc that results in such structuring. However, it is worth noting that there have been observations of substorm onset arcs that do not show signatures of auroral beads (Angelopoulos et al., 2008; Nishimura et al., 2010).

As to their source, Motoba et al. (2012) showed conjugate observations of beads in both hemispheres, suggesting that beads are the result of a magnetospheric, and not an ionospheric, phenomenon. Rae et al. (2010) presented the first detailed optical analysis of large-scale auroral beads, demonstrating that the growth of low azimuthal wave numbers was approximately exponential. They concluded that beads were the optical manifestation of a magnetospheric instability. More recently, Kalmoni et al. (2015) presented a statistical study of 17 auroral bead events, confirming that auroral brightness grew exponentially over a range of spatial scales and that the beads were the ionospheric counterpart of a magnetospheric plasma instability. Mapping auroral beads from the ionosphere into the magnetotail suggests that the source region lies between ~8 and 12 R_E from the Earth (Donovan et al., 2008; Kalmoni et al., 2015, 2018).

The aim of this work is to present a statistical survey of ULF magnetic field fluctuations in the near magnetotail, associated with auroral beads in the interval around substorm onset. Section 2 describes the data and methods along with an example showing conjugate observations of the growth of ULF wave power and auroral images showing the development of auroral beads. Section 3 compares the results from the ground and space based observations around substorm onset, in terms of timing and the properties of the growth of ULF wave power. The observations of large wave power in the magnetotail are then examined relative to their timing and location. The results are then discussed in section 4, before a summary is presented in section 5.

2. Data and Methodology

The Time History of Events and Macroscale Interactions during Substorms (THEMIS) mission provides a combination of ground-based observatories coupled with five orbiting spacecraft designed to investigate magnetospheric substorms (Angelopoulos, 2008). In this work we use data from three orbiting spacecraft, specifically the magnetometers (Auster et al., 2009) and electrostatic analyzers (McFadden et al., 2009) on board the THEMIS A, D, and E spacecraft. The low-resolution (4 Hz) magnetic field data and reduced resolution (0.33 Hz) plasma moments are used. We also use concurrent data from the THEMIS all-sky imagers (ASIs) (Mende et al., 2008) and magnetometers (Russell et al., 2008; Mann et al., 2008). The ASI network initially consisted of 20 white light cameras spread over the North American continent, recording images with a 3 s time and 256×256 pixel resolution. The ground-based magnetometer data are used at 2 Hz resolution.

To perform the survey we first use a list of substorm expansion phase onsets provided by the SOPHIE technique (Forsyth et al., 2015). The SOPHIE method uses the derivatives of the SuperMAG SMU and SML indices (Gjerloev, 2009, 2012) to identify the three phases of substorms. The technique identifies those intervals exceeding percentiles of the derivatives of SML (expansion percentile thresholds, EPTs) in order to select small or large rates of change as required. In this work we employ the 90th percentile (EPT = 90), selecting

expansion phase onsets associated with top 10% rates of change of the SML index. Forsyth et al. (2015) found that using the 75th percentile (EPT = 75) gave a good agreement between SOPHIE and auroral onset lists; however, some events such as large pseudo-breakups may also be included. Using an EPT of 90 tends to identify substorms with larger magnetic bays, but should also reduce false identifications.

To explore and identify wave activity we require a frequency or period band on which to concentrate. Studies of ULF waves around substorm onset commonly use the wave bands identified by Jacobs et al. (1964). Historically the most commonly used period bands for ground-based substorm studies have been the Pi1 (1–40 s) and Pi2 (40–150 s) bands. Pi2 band fluctuations have long been known to be present at the beginning of magnetic bays (Angenheister, 1913; Saito, 1969) and were initially thought only to be related to the diversion of the cross-tail current into the ionosphere (Atkinson, 1967; Lester et al., 1983; McPherron et al., 1973) and flows within the plasma sheet (Kepko & Kivelson, 1999; Murphy et al., 2011). Pi1 period waves, with their shorter periods, are often observed at similar times to the Pi2 pulsations (Bosinger & Yahnin, 1987; Jacobs et al., 1964). More recent work has often used a combination of the two period bands, often denoted Pi1-2 and spanning the period band 24–96 s (e.g., Milling et al., 2008; Murphy et al., 2009; Rae et al., 2011, 2017), which have been shown to be coincident with auroral beads (Rae, Mann, Murphy, et al., 2009; Walsh et al., 2010). Additionally, the spectra of ULF waves around substorm onset has been shown to be a power law, with no clear break separating the Pi1 and Pi2 wave bands (Murphy et al., 2011). In this study we use a slightly wider period band, 10–100 s to capture those periods observed on the ground while also considering that the ionosphere may screen some lower period fluctuations which may be seen in space.

2.1. Example Interval: 31/03/09

Figure 1 shows an interval around substorm expansion phase onset from ground- and conjugate space-based instrumentation on 31 March 2009. Figures 1a–1d show four ASI images from the Fort Smith (FSMI) station, showing the brightening auroral arc. The images have been mapped to an altitude of 110 km and are presented on a grid of geographical latitude and longitude; elevation angles below 10° have not been plotted. The bright static spot on the left of the images is the moon. Azimuthal structure is clearly visible in the brightening arc, that is, the development of auroral beads. During this interval, the THEMIS A, D, and E spacecraft were located at approximately $X_{GSM} \sim -11R_E$ and with Y_{GSM} ranging between 2.5 and $3.5R_E$ (i.e., premidnight). These locations map (using the Tsyganenko & Sitnov, 2005, model, henceforth TS05) to points at the right of Figures 1a–1d, within the brightening arc. The mappings for THEMIS A and E overlap.

The lower panels (Figures 1e–1h) show 45 min of data starting 30 min before the SOPHIE-identified expansion phase onset and ending 15 min post SOPHIE onset. The SOPHIE onset at 06:26 UT is indicated with a vertical red dashed line, while the timings of Figures 1a–1d are indicated with vertical dashed blue lines. The SML data from which the SOPHIE onset has been identified are provided in Figure 1i. Figure 1e shows a north-south keogram from the FSMI station, zoomed into the region of the keogram showing the auroral arc. The auroral arc can be seen to brighten substantially starting around 06:20 UT, followed by some poleward (northward) motion.

Figure 1f shows the integrated brightness of the FSMI ASI shown on a logarithmic scale as a function of time, to indicate the relative timing of the exponentially brightening arc. Figure 1g shows the squared horizontal component of the ground magnetic field, filtered between 10 and 100 s. The data have been Hilbert transformed and the amplitude envelope of the oscillations extracted. The individual components have been combined in quadrature and squared to provide a measure of the wave power in the fluctuations. It can be seen that during the brightening of the arc, the ground magnetic field perturbations between 10 and 100 sincrease by approximately two orders of magnitude. The time of peak ground ULF power is indicated with a black vertical dashed line.

Figure 1h shows the contemporaneous in situ magentic field recorded by the THEMIS A, D, and E spacecraft. As with Figure 1g, each component of the magnetic field has been filtered between 10 and 100 s, Hilbert transformed, and combined in quadrature; the square of which is plotted as a measure of the ULF power. There is a clear exponential increase of greater than three orders of magnitude of ULF power in the period band of interest, coinciding with the auroral brightening and ground magnetic field power increase. Fitting exponentials to the increases in wave power measured on the ground and in space reveals rates of 0.01–0.02 s^{-1}. It is also interesting to note that the growth of ULF power precedes the time of SOPHIE onset, suggesting that the large-scale current systems form after the wave growth. This paper concerns a survey

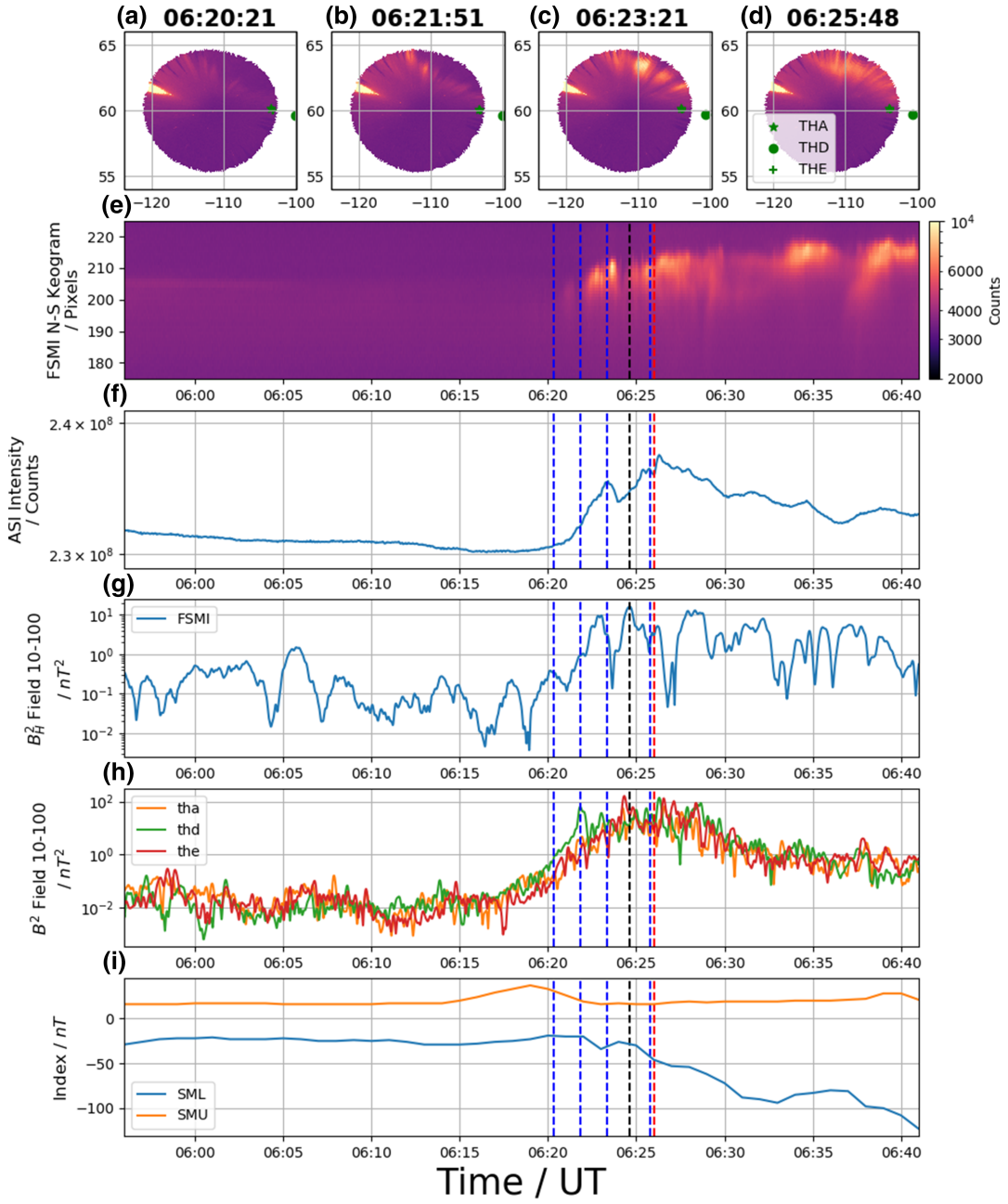

Figure 1. Observations around substorm onset on 31/03/09 from 05:56 to 06:41. Top row (a–d): four images taken around onset by the FSMI (Fort Smith) ASI; the relative timings of which are indicated with blue vertical dashed lines in the lower panels. The THEMIS A, D, and E spacecraft locations are shown mapped to the images in green using the Tsyganenko and Sitnov (2005) model. The lower panels show: a north-south keogram from FSMI (e); the integrated brightness from the FSMI images (f); the squared horizontal component of the ground magnetic field at FSMI filtered between periods of 10 to 100 s (g); the squared total magnetic field observed by THEMIS A, D, and E, once more filtered between 10 and 100 s (h); and the SML and SMU indices (i). The vertical dashed black and red lines indicate the peak of the filtered ground magnetic field and the substorm onset from the SOPHIE catalog (Forsyth et al., 2015), respectively.

of spacecraft data, exploring the presence, timing, and location of such increases in wave power using the same methodology as shown in Figure 1.

2.2. Spacecraft Coverage

We use data obtained during the 2009 THEMIS tail season, specifically between 15 January 2009 and 30 April, a period during which the THEMIS A, D, and E spacecraft sampled the near-Earth plasma sheet while largely mapping to regions covered by the THEMIS ground stations.

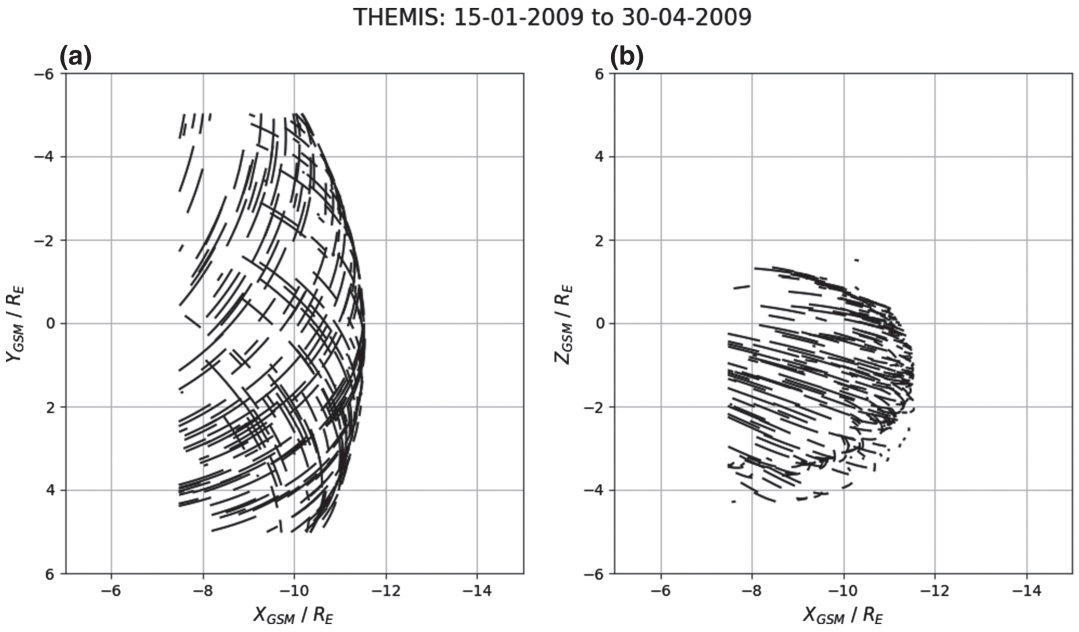

Figure 2. The distribution of THEMIS A, D, and E spacecraft orbits within $-12.5 \leq X_{GSM} \leq -7.5R_E$ and $-5 \leq Y_{GSM} \leq 5R_E$ where the $\beta \geq 1$. Only data within ±30 min from SOPHIE expansion phase onset are plotted.

As described above, we use a catalog of expansion phase onsets created using the SOPHIE method (Forsyth et al., 2015). In total, 506 onsets occurred within the time interval considered by the study. Occasionally the SOPHIE catalog reports several onsets separated by a few tens of minutes. As we are interested in the relative timing of large wave power compared to substorm onset, we remove such intervals by placing a requirement that each onset must be preceded by at least 90 min of quiet (i.e., with no other onset present). This leaves a total of 335 isolated onsets in the time interval (66% of the total).

With these as the starting point, we explore THEMIS A, D, and E spacecraft data in the time ±60 min from the SOPHIE onset. Previous works have either mapped auroral beads into the magnetotail or observed ULF fluctuations in the magnetotail inferred to be related to beads; both methods have typically located the phenomena between ~8 and 12 R_E downtail (e.g., Chang & Cheng, 2015; Donovan et al., 2008; Kalmoni et al., 2015, 2018). We therefore define a broad region of interest to identify intervals of spacecraft data for further investigation:

- $-12.5 \leq X_{GSM} \leq -7.5R_E$
- $-5 \leq Y_{GSM} \leq 5R_E$
- $-5 \leq Z_{GSM} \leq 5R_E$

All magnetospheric phenomena suggested to be responsible for beads occur within the plasma sheet (e.g., Lui et al., 1991; Voronkov et al., 1997), and we therefore require that the spacecraft are within the plasma sheet ($\beta \geq 1$) (cf. Angelopoulos et al., 1994). After performing the described selection process, a total of 176 onsets remain during which at least one spacecraft was within the region of interest. This corresponds to 471 intervals of spacecraft data, which form the dataset for this study. Figure 2 shows the distribution of data in the $X_{GSM} - Y_{GSM}$ plane (a) and $X_{GSM} - Z_{GSM}$ plane (b).

3. Results

We now explore the presence, location, and properties of increased ULF wave power around substorm onset.

3.1. Superposed Epoch Analysis: Ground and Space Comparison

First, we examine the relative timing of elevated wave power using superposed epoch analysis (SEA). For this analysis, the events are aligned to a time T_0, with a consistent physics-based definition between the individual time series. We could define T_0 as the time identified by SOPHIE as representing expansion phase onset, which would yield a repeatable and quantitatively defined epoch based on the SML index. However, SOPHIE

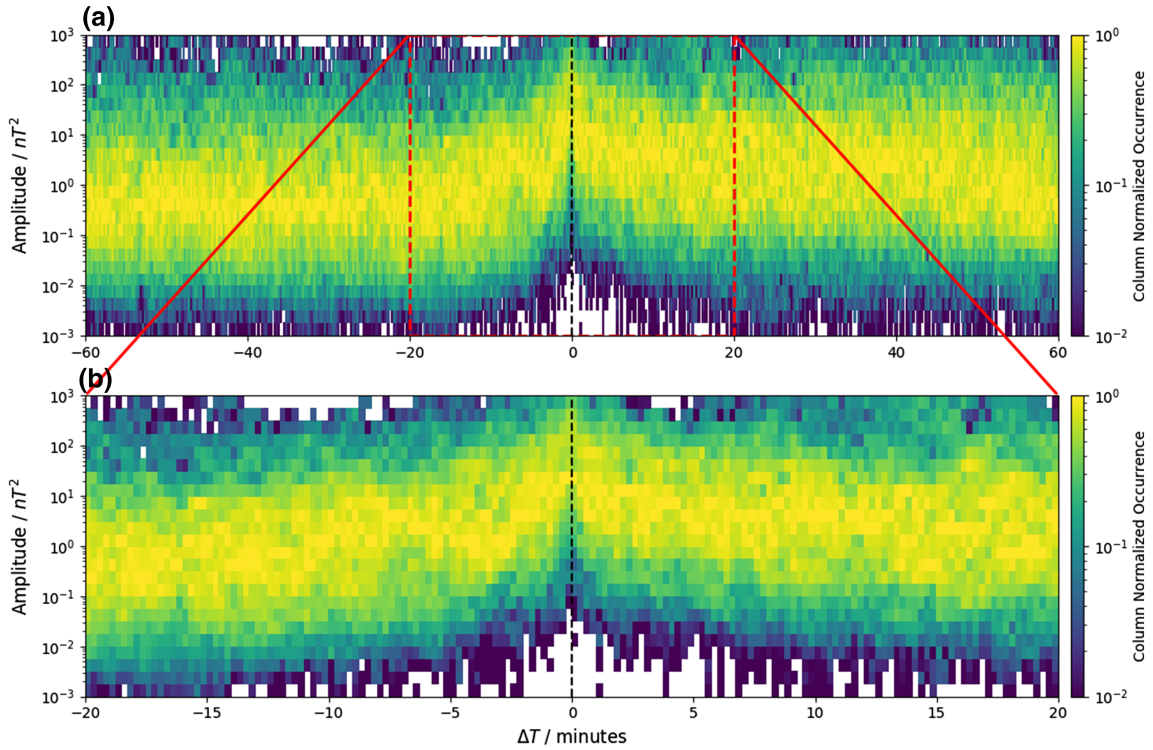

Figure 3. A superposed epoch analysis (SEA) of the closest ground station to the mapped spacecraft locations during substorms, plotted for ±60 min (a) and ±20 min (b). T_0 is defined as the peak of the ground wave power. The wave power amplitudes were calculated with the same method as presented in section 2.1 and Figures 1g and 1h.

has been shown to follow auroral-defined onsets (e.g., the onsets of Frey et al., 2004; Frey & Mende, 2006), with the distribution of time differences showing a full width at half maximum (FWHM) of 13 min (Forsyth et al., 2015). We therefore define T_0 as the peak wave power (in the 10–100 s period band) as measured by the closest ground station to the mapped spacecraft location, using the TS05 model. In the example event in Figure 1, T_0 is indicated by the vertical dashed black line. A period ±10 min of SOPHIE onset is considered to locate the peak ground wave power. It should be noted that the peak in the conjugate ground station may not correspond exactly to the substorm onset time as defined by auroral breakup. Pi1-2 wave power has been observed to spread from an epicenter (e.g., Milling et al., 2008; Murphy et al., 2009), coincident with auroral fluctuations several minutes prior to auroral breakup (e.g., Rae, Mann, Angelopoulos, et al., 2009; Rae, Mann, Murphy, et al., 2009; Rae et al., 2010). However, the choice of T_0 based on the peak of the conjugate ground ULF power provides a consistent and repeatable baseline with which to align the space-based observations.

Figure 3 shows the results of a superposed epoch analyses of the ground station data around the peak measured ULF power; the data were prepared with the same steps as were used in Figure 1g. Rather than presenting the average wave power at each epoch, we show the distribution of wave powers at each time step due to the observed wave powers varying by five orders of magnitude or more. It is clear from Figure 3a that there is an increase in the power of the fluctuations around T_0 of several order of magnitude. Broadly, the ULF power in the SEA can be seen to rise around 5–10 minutes prior to the peak and decay more slowly following T_0.

Figure 4 shows an SEA of the ULF power observed by the in situ spacecraft; the data have been processed with the same method as above, though all three components (B_X, B_Y, B_Z) of the magnetic field have been considered. Figure 4 looks remarkably similar in shape to Figure 3, with a clear peak in the ULF power around T_0. Likewise, the increase in ULF power appears to start around 5–10 min prior to T_0 and decay over the following 20 min. The precise growth rates and relative timings observed are examined in more detail below.

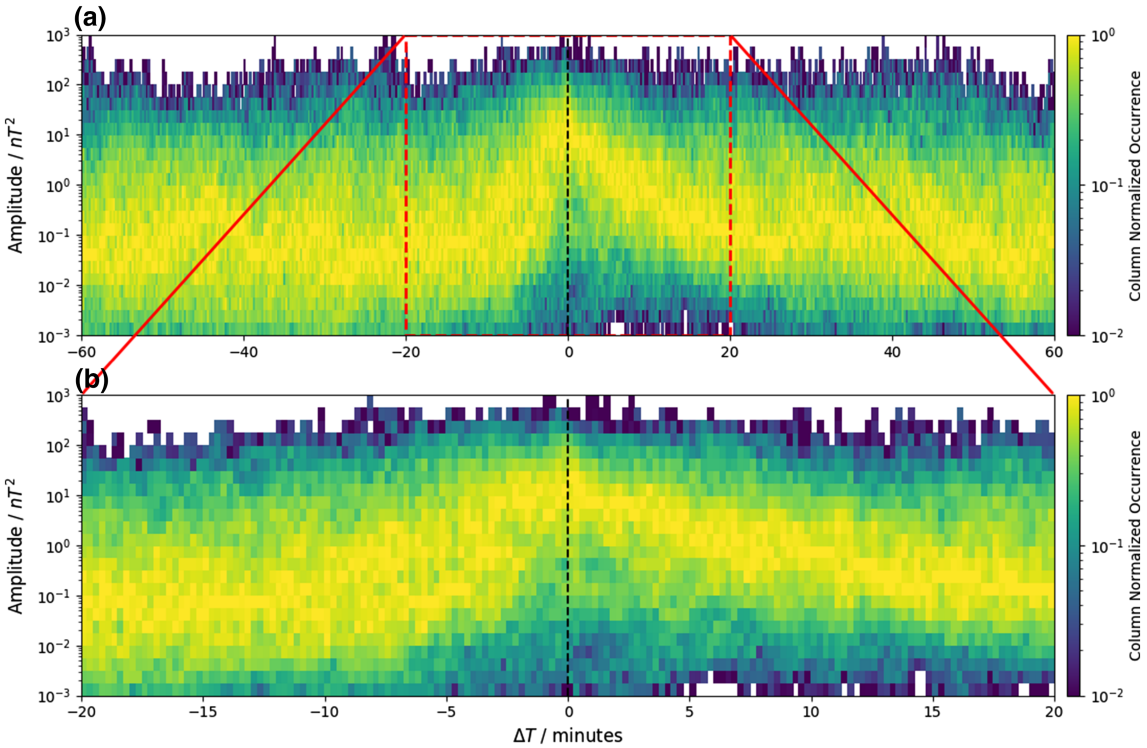

Figure 4. A superposed epoch analysis (SEA) of the spacecraft data during substorms. T_0 is defined as the peak in the wave power of the closest ground station to the mapped spacecraft location. The format is the same as Figure 3.

3.2. Properties of Exponential Wave Power Growth

Thus far, the results presented have suggested the existence of conjugate, exponential increases in wave power on the ground and in the near-Earth magnetotail plasma sheet. We now examine the growth rate of power during each individual event, along with the duration and relative timing of the growth.

First, we manually identified intervals of exponential growth in both the ground and spacecraft data related to the SOPHIE onsets. Section 2.2 described the process by which intervals were selected, with a total of 176 SOPHIE onsets during which at least one spacecraft within the near-Earth magnetotail plasma sheet. For each of these onsets, the spacecraft were mapped to the ground (with the TS05 model) and the closest magnetometer station identified. From this data set, 117 ground stations (66% of the total) show clear exponential growth in wave power leading to a peak wave power within ±10 min of the SOPHIE onset time. The subset for which exponential growth was not observed (59 onsets, 34% of the total) may simply have been in the wrong spatial location to observe such a signature at onset, for example, mapping to postmidnight in the magnetotail (cf. Figure 7). Meanwhile, within the near-Earth magnetotail plasma sheet, 203 intervals (out of 471, 43%) of spacecraft data show clear exponential increases in wave power. Of these 203 intervals, 175 (86%) can be matched to the previously discussed, conjugate, and independently identified intervals of exponential growth on the ground. It should be noted that during the identification process, data around SOPHIE onset were examined individually without knowledge as to the source of the data (i.e., the spacecraft or ground station) and with only the SOPHIE onset time marked for reference.

We then fit exponential functions to each identified period of wave power growth, using an orthogonal distance regression technique and fitting a linear equation to the logarithm of the wave power. Performing this analysis on the event in Figure 1 returned growth rates between 0.014 s^{-1} and 0.023 s^{-1}. Figure 5 displays histograms of the fitted growth rate (left column) and the duration of the exponential growth interval (right column), for the space- (top row) and ground-based data (lower row). Comparing the upper and lower panels confirms the suggestion made in Section 3.1 that both the ground and space show similar periods of exponential wave power growth. The mean and median growth rates are on average found to be ~0.01 s^{-1} in both locations, while the exponential growth lasts for ~4–5 min on average.

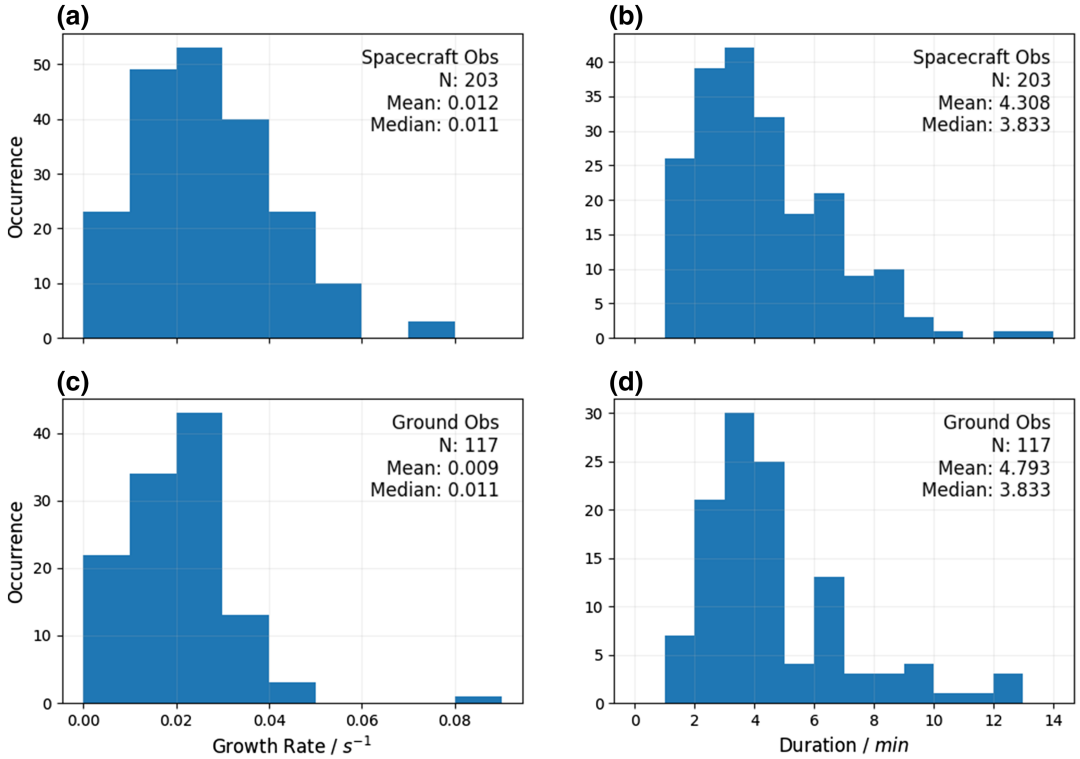

Figure 5. The properties of the intervals of exponential wave power growth from the THEMIS spacecraft (a, b) and conjugate ground based observatories (c, d). The left column (a, c) shows histograms of the growth rates, while the right (b, d) shows histograms of the duration of the exponential growth.

We are also interested in the relative timing of such exponential growth of wave power. To investigate, we take the 117 periods of exponential growth identified in the ground based data and cross-correlate them with the 175 intervals of conjugate spacecraft data that exhibited exponential growth. We cross-correlate the logarithm of wave power as the wave power changes over orders of magnitude. We once more limit this to intervals when the spacecraft are within the region of interest. Figure 6a shows the resulting maximum Pearson coefficients for the cross-correlation, tested for lags of ±600 s. Figure 6b shows the lags of maximum correlation, limited to those comparisons with a Pearson coefficient above 0.8. Overall, there are 137 (78% of the 175) intervals of spacecraft data that correlate with the exponential increase in ground wave power with a Pearson coefficient above 0.8, the mean and median lags of which are −89 and −51 s, respectively. It should be noted that changing the threshold on the Pearson coefficient (e.g., reducing it to 0.7, or increasing it to 0.9) does not effect the distribution of times, mean, or median significantly. The predominantly negative lags indicate that the exponential increase in wave power on the ground most often occurs after the corresponding exponential interval in the space based data. Therefore, the signatures in space are on average 1–1.5 min ahead of those on the ground. It should be noted that the time differences will also include a factor accounting for the spatial difference between the mapped spacecraft and the ground station. The mean distance between the mapped footpoint of the spacecraft and the closest THEMIS ground station is 435 km, with a standard deviation of 560 km. This broad distribution reflects the separation of the THEMIS ground stations and explains the spread of time differences observed.

3.3. Spatial Distribution

In addition to investigating the relative timing of the ULF wave power increase, we are also interested in the location of enhanced ULF wave power observations within the magnetotail.

We therefore require a definition of enhanced wave power. In this work we define enhanced as exceeding a large percentile of the background wave power in the magnetotail, that is, that observed at times unrelated to substorm onset. We select data recorded between 30 and 90 min prior to the SOPHIE onsets included in this study as our background dataset, within the region of interest defined in section 2.2. Figure 7a shows the percentage of space-based wave power observations that exceed three selected percentiles of the background

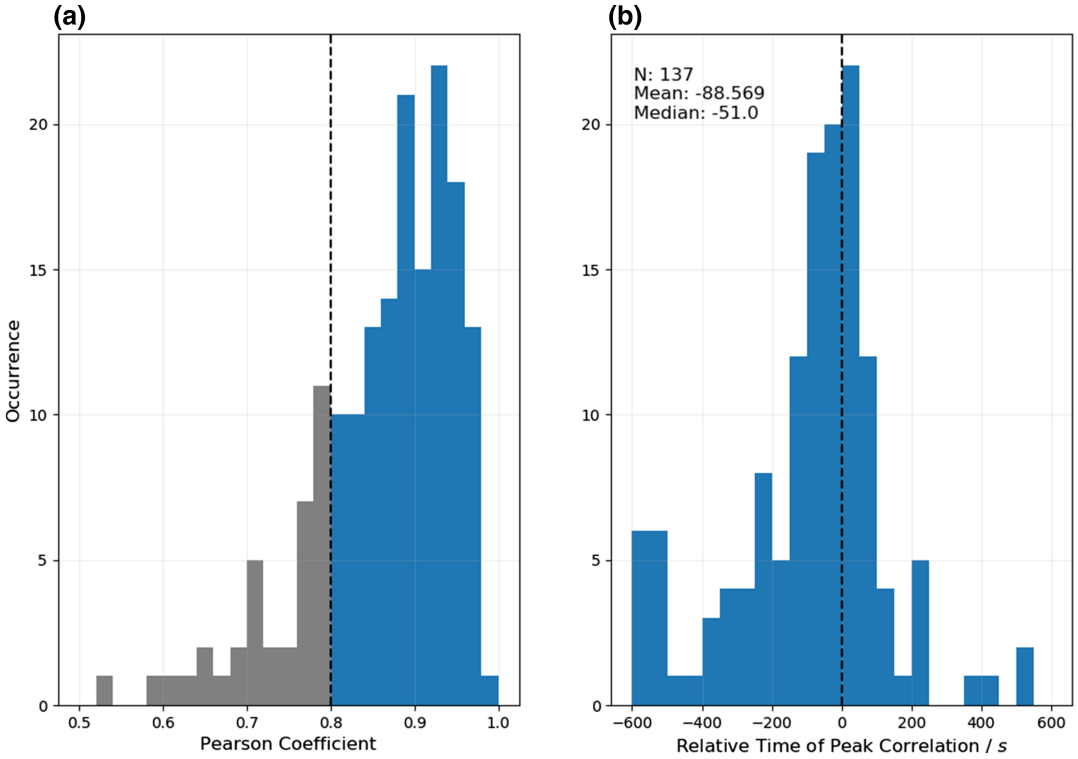

Figure 6. Results of cross-correlating the exponential increases in ground wave power with the THEMIS satellite observations of wave power. (a) A histogram of the 175 maximum Pearson coefficients and (b) the relative times corresponding to the 137 intervals with Pearson coefficients above 0.8.

dataset. The 90th (blue), 99th (orange), and 99.9th (green) percentiles represent significant enhancements of ULF wave power and correspond to 2.8 nT^2, 31.6 nT^2, and 136.7 nT^2, respectively.

First, from Figure 7a, it is clear that the percentage of data above all three thresholds is greatest in the few minutes around T_0. All three percentiles show an increase towards this peak starting between 10 and 15 min prior to T_0. The occurrence then subsides over a similar 10–15 min time scale. At the peak, just prior to T_0, 56% of recorded wave power exceeds the 90th percentile of the background, while 18% and 3% exceed the 99th and 99.9th percentiles of the background, respectively.

Figures 7b–7i display 2-D histograms of the percentage of data recorded that exceeds the 99th (b–e) and 99.9th (f–i) percentiles of the background wave power, binned by spacecraft location. Each column in the lower panels represents data within a 5 min time window relative to T_0. Regions with no observations or no observations above the given percentile of the background wave power are shown in white.

Figures 7b–7i show a large dawn-dusk asymmetry: Larger percentages of the observations show ULF wave power exceeding the 99th and 99.9th percentiles of the background on the premidnight side of the tail. Initially, 10–15 min prior to the peak ground ULF power (Figure 7b), fewer than 10% of the observations of ULF wave power are greater than the 99th percentile of the background, with the majority located premidnight. Meanwhile, observations of ULF power above the 99.9th percentile of the background are very rare (representing ~1% of observations) in few spatial regions (Figure 7f). Moving closer to onset, up to 5 min before T_0 (Figures 7c and 7g), around 10% of observations at and before midnight are above the 99th percentile of the background, while ULF wave power exceeding the 99.9th percentile of the background is still rare (1% of observations). Then, in the few minutes before T_0, 10–30% of observations in the premidnight region exceed the 99th percentile of the background, and up to 10% exceed the 99.9th (Figures 7d and 7h). Finally, in the 5 min following T_0 (Figure 7e), between 10% and 20% of the premidnight tail observes ULF power greater than the 99th percentile of the background, while the distribution is similar to the previous 5 min interval.

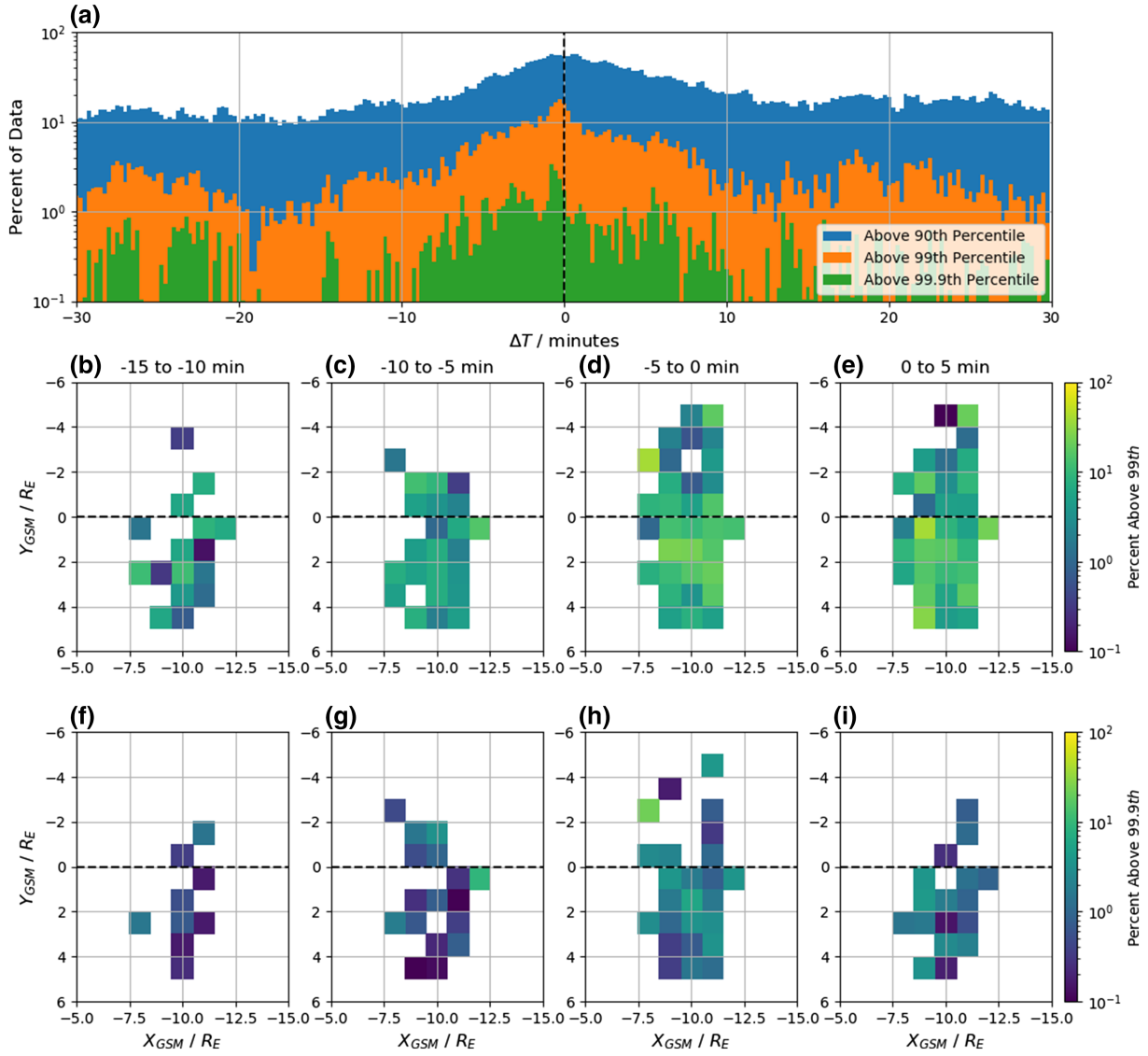

Figure 7. The percentage of space-based observations of wave power that exceed the 90th (blue), 99th (orange), and 99.9th (green) percentiles of the background wave power as a function of time from T_0, plotted for ±30 min (a). The percentage of data exceeding the 99th (b–e) and 99.9th (f–i) percentile of the background wave power across the magnetotail for a series of 5 min intervals relative to T_0.

4. Discussion

Substorm onset is a notoriously difficult topic, with complex and interconnected physical processes operating over a very large spatial domain. In this work we have focused on a repeatable signature of substorm onset: the exponential growth of ULF wave power. This increase in ground ULF wave power has been shown to spread coherently from an epicenter, colocated with the location of auroral onset (Milling et al., 2008; Murphy et al., 2009). Meanwhile, the rapid increases in ULF wave power have been linked to azimuthal structuring of the onset arc, as measured by coincident ground based ASI stations (Rae, Mann, Angelopoulos, et al., 2009; Rae, Mann, Murphy, et al., 2009; Rae et al., 2010, 2012; Sakaguchi et al., 2009). While wave-like activity with periods between ~20 and 100 s has been observed around substorm onset in the magnetotail (e.g., Angelopoulos et al., 2002; Chang & Cheng, 2015, Chaston et al., 2012; Ergun et al., 2015; Keiling, 2012; Lui et al., 2008; Motoba et al., 2015; Panov et al., 2012; Saito et al., 2008; Uritsky et al., 2009; Walsh et al., 2010), here, we have presented the first statistical study.

Pi2 pulsations, with periods between 40 and 150 s (Jacobs et al., 1964), have long been thought to be related to field-aligned currents generated at onset (e.g., Olson, 1999, and references therein). In particular, the

polarization of Pi2s has been shown to provide information about the location of the substorm current wedge (e.g., Lester et al., 1983). However, Milling et al. (2008) used discrete wavelet transforms to show that in fact the first period band to rise above a predetermined noise threshold at substorm onset was the 12–48 s period band, combining the low period Pi2 with the upper part of the Pi1 range (periods between 1 and 40 s). Later work with a larger number of events showed that either the 12–48 s or 24–96 s band was the first to rise above the specified noise level (Murphy et al., 2009; Rae, Mann, Murphy, et al., 2009). With this in mind, in this work, we have used a broader 10–100 s period band than in earlier work; we have attempted to capture the whole frequency range of substorm-related oscillations.

In performing this statistical study we have made several key assumptions, the first of which is that the rapid increase in ULF wave power is a universal signature of onset and that it is linked to the spatially and temporally coincident azimuthal structuring of the auroral arc: auroral beads (e.g., Rae et al., 2010). This first assumption allows us to use an independently derived list of substorms (Forsyth et al., 2015), around which to begin the investigation. We have also assumed that the ULF wave power and auroral beads have a magnetospheric and not an ionospheric source (Sakaguchi et al., 2009; Kataoka et al., 2011; Motoba et al., 2012). Finally, given that there is a magnetospheric source, we have assumed that the source provides a repeatable signature of increasing ULF wave power in this region.

The case study example in Figure 1 showed a period of exponential growth in magnetotail ULF power that slightly preceded the increases in ground ULF power and integrated auroral brightness. Concurrent all-sky imagery also showed the presence of auroral beads within the brightening arc. The exponential growth of ULF wave power in space can be seen to start approximately 10 min prior to the peak ground ULF power. Figures 3 and 4 then showed superposed epoch analyses of the ground- and conjugate space-based ULF wave power around the time of maximum ground wave power, which appear remarkably similar. This confirms that significant magnitude ULF waves in the 10–100 s period band are commonly present on both the ground and in the magnetotail with very similar timings around substorm onset. Figure 6 further quantified the relative timing between the ground- and space-based observations, showing that on average, the ground observations lagged those in space by approximately 1–1.5 min on average. A time scale of a few minutes would be consistent with communication from the magnetotail to the ground by MHD waves (e.g., Chi et al., 2009; Ferdousi & Raeder, 2016). If shear Alfvén waves of short perpendicular scale are involved, as the case study of auroral beads by Kalmoni et al. (2018) suggests, they may be responsible for the auroral acceleration, as suggested by Mende et al. (2003). Watt and Rankin (2010) and Watt and Rankin (2012) have shown that if shear Alfvén waves have short perpendicular scales in the plasma sheet, then they can be responsible for acceleration that would produce visible aurora.

Figure 5 examined the details of the exponential increases in wave power, finding an average growth rate of $\sim 0.01\ s^{-1}$ both on the ground and in space, while the increase in wave power generally occurred over a period between 1 and 12 minutes. These growth rates are smaller than those observed from prior optical analyses of 17 cases of auroral beads, where growth rates of auroral brightness at different spatial scales ranged from $0.03–0.3\ s^{-1}$ (Kalmoni et al., 2015). The discrepancy could be a result of the broad period band pass (10–100 s) considered in this study; the growth rates observed in the development of auroral beads depend heavily on the spatial scale (Kalmoni et al., 2015, 2018; Rae et al., 2010). Recently, Kalmoni et al. (2018) associated the azimuthal structuring of the onset arc with kinetic Alfvén waves with short perpendicular scales driven by a process within the magnetotail plasma sheet. The waves could be those driven unstable in the plasma sheet or could be the oscillations communicating the presence of the instability from the plasma sheet, along the field to the ionosphere. Possible sources of free energy that could drive the instability included pressure gradients (Kistler et al., 1992; Nagai et al., 1997; Sun et al., 2017; Xing et al., 2010), shear flows (Samson et al., 2003; Viñas & Madden, 1986; Voronkov et al., 1997), and electron temperature anisotropies (Walsh et al., 2011).

Figure 7 showed that observations of large ULF power are much more likely premidnight in the minutes leading up to the peak ground ULF wave power. Many dawn-dusk asymmetries are observed in the Earth's magnetotail (e.g., Walsh et al., 2014, and references therein); for example, magnetotail current density is consistently higher (e.g., Artemyev et al., 2011; Runov et al., 2005), and thin current sheets are more common on the dusk/premidnight side of the tail (e.g., Rong et al., 2011). Our observations also closely mirror

the premidnight preference for substorms (Frey et al., 2004; Frey & Mende, 2006) and substorm-related phenomena and structures, such as those linked with reconnection (Imber et al., 2011; Nagai et al., 2013; Slavin et al., 1985, 2005).

5. Summary

In this paper, we first presented a case study, showing the development of auroral beads in the pre-onset auroral arc. The exponentially brightening ASI images were shown to be concurrent with an exponential increase in ULF power in the 10–100 s period band of the horizontal ground magnetic field. Data from three conjugate THEMIS spacecraft, located at a radial distance of approximately $10R_E$, also observed clear exponential increases in ULF power in the 10–100 s period band.

We then showed a statistical survey of ULF power in the magnetotail around substorm onset. We selected isolated substorm onsets identified independently using the SOPHIE method (Forsyth et al., 2015), selecting those onsets for which at least one of the THEMIS spacecraft were within the near-Earth magnetotail plasma sheet. Superposed epoch analyses were then presented showing conjugate ground- and space-based observations of ULF power, aligned to the peak in the ground station ULF power. Both plots were remarkably consistent, with clearly increasing ULF wave power present in both regions up to 10 min prior to the peak in ground ULF power.

Clear intervals of exponential growth of ULF wave power were then manually identified in both the THEMIS spacecraft and conjugate ground-based data. The resulting exponential fits provided consistent average growth rates of $\sim 0.01\ s^{-1}$, with the exponential growth lasting for intervals between approximately 1 and 12 min. This average growth rate is lower than the scale-dependent growth rate inferred from optical observations of auroral beads; this could be the result of the broad band pass filtering applied. The identified exponential growth intervals in the ground-based dataset were cross-correlated with the conjugate space-based observations. A total of 137 intervals of spacecraft data correlated with the ground with a Pearson coefficient greater than 0.8; on average, these observations lead the ground observations by approximately 1–1.5 min. Further, observations of ULF power above the 99th and 99.9th percentile of quiet levels were examined as to their location. A clear preference for premidnight observations were shown, at radial distances of approximately $10R_E$.

Overall, these findings suggest that the linear phase of a magnetospheric instability is active in the premidnight region of the magnetotail for several minutes prior to substorm onset. This instability causes conjugate ULF wave activity on the ground with approximately a 2 min delay, likely linked to simultaneous and coincident azimuthal structuring of the auroral arc.

Acknowledgments
We acknowledge NASA contract NAS5-02099 and V. Angelopoulos for use of data from the THEMIS Mission. Specifically: C. W. Carlson and J. P. McFadden for use of ESA data; K. H. Glassmeier, U. Auster, and W. Baumjohann for the use of FGM data provided under the lead of the Technical University of Braunschweig and with financial support through the German Ministry for Economy and Technology and the German Center for Aviation and Space (DLR) under contract 50 OC 0302; S. Mende and E. Donovan for use of the ASI data, the CSA for logistical support in fielding and data retrieval from the GBO stations, and NSF for support of GIMNAST through grant AGS-1004736; and S. Mende and C. T. Russell for use of the GMAG data and NSF for support through grant AGS-1004814; I. R. Mann, D. K. Milling, and the rest of the CARISMA team for use of GMAG data. CARISMA is operated by the University of Alberta, funded by the Canadian Space Agency (http://www.carisma.ca/); Data provided by the Geophysical Institute Magnetometer Array operated by the Geophysical Institute, University of Alaska is available at https://www.gi.alaska.edu/monitors/magnetometer/archive. THEMIS data are available at: http://themis.ssl.berkeley.edu/data/themis/. The SuperMAG geomagnetic indices can be found at http://supermag.jhuapl.edu. A. W. S. and I. J. R. were supported by STFC Consolidated Grant ST/S000240/1 and NERC Grant NE/P017150/1. C. F. was supported by the NERC Independent Research Fellowship NE/N014480/1 and STFC Consolidated Grant ST/S000240/1. C. E. J. W. was supported by STFC Consolidated Grant ST/R000921/1 and NERC Grant NE/P017274/1. K. R. M. is supported by the NSF Grant 1602403. The analysis in this paper was performed using python, including the pandas, numpy, scipy, cartopy, and matplotlib libraries.

References

Akasofu, S. I. (1964). The development of the auroral substorm. *Planetary and Space Science*, *12*(4), 273–282. https://doi.org/10.1016/0032-0633(64)90151-5

Akasofu, S. I. (1977). Physics of magnetospheric substorms. *Research supported by NSF, NASA, ERDA, and U.S. Air Force. Dordrecht, D. Reidel Publishing Co. (Astrophysics and Space Science Library. Volume 47), 1977. 619 p.*, https://adsabs.harvard.edu/abs/1977nsf....47.....A

Akasofu, S. I., & Chapman, S. (1961). The ring current, geomagnetic disturbance, and the Van Allen radiation belts. *Journal of Geophysical Research*, *66*(5), 1321–1350. https://doi.org/10.1029/JZ066i005p01321

Angelopoulos, V. (2008). The THEMIS mission. *Space Science Reviews*, *141*(1-4), 5–34. https://doi.org/10.1007/s11214-008-9336-1

Angelopoulos, V., Chapman, J. A., Mozer, F. S., Scudder, J. D., Russell, C. T., Tsuruda, K., & Yumoto, K. (2002). Plasma sheet electromagnetic power generation and its dissipation along auroral field lines. *Journal of Geophysical Research*, *107*(A8), 1181. https://doi.org/10.1029/2001JA900136

Angelopoulos, V., Kennel, C. F., Coroniti, F. V., Pellat, R., Kivelson, M. G., Walker, R. J., & Gosling, J. T. (1994). Statistical characteristics of bursty bulk flow events. *Journal of Geophysical Research*, *99*(A11), 21,257. https://doi.org/10.1029/94JA01263

Angelopoulos, V., McFadden, J. P., Larson, D., Carlson, C. W., Mende, S. B., Frey, H., & Kepko, L. (2008). Tail reconnection triggering substorm onset. *Science (New York, N.Y.)*, *321*(5891), 931–5. https://doi.org/10.1126/science.1160495

Angenheister, G. (1913). Ueber die Fortpflanzungsgeschwindigkeit magnetischer Störungen und Pulsationen. Bericht über die erdmagnetischen Schnellregistrierungen in Apia (Samoa), Batavia, Cheltenham und Tsingtau im September 1911. *Nachrichten von der Gesellschaft der Wissenschaften zu Göttingen, Mathematisch-Physikalische Klasse*, 1913, 565–581. https://eudml.org/doc/58893

Artemyev, A. V., Petrukovich, A. A., Nakamura, R., & Zelenyi, L. M. (2011). Cluster statistics of thin current sheets in the Earth magnetotail: Specifics of the dawn flank, proton temperature profiles and electrostatic effects. *Journal of Geophysical Research*, *116*, A09233. https://doi.org/10.1029/2011JA016801

Atkinson, G. (1967). The current system of geomagnetic bays. *Journal of Geophysical Research*, *23*, 6063–6067. https://doi.org/10.1029/JZ072i023p06063

Auster, H. U., Glassmeier, K. H., Magnes, W., Aydogar, O., Baumjohann, W., Constantinescu, D., & Wiedemann, M. (2009). The THEMIS fluxgate magnetometer, *The THEMIS Mission* (pp. 235–264). New York, NY: Springer New York. https://doi.org/10.1007/978-0-387-89820-9_11

Baker, D. N., Pulkkinen, T. I., Angelopoulos, V., Baumjohann, W., & McPherron, R. L. (1996). Neutral line model of substorms: Past results and present view. *Journal of Geophysical Research*, *101*(A6), 12,975–13,010. https://doi.org/10.1029/95JA03753

Bosinger, T., & Yahnin, A. (1987). Pi1B type magnetic pulsation as a high time resolution monitor of substorm development. *Annales Geophysicae*, *5*, 231–237.

Chang, T. F., & Cheng, C. Z. (2015). Relationship between wave-like auroral arcs and Pi2 disturbances in plasma sheet prior to substorm onset. *Earth, Planets and Space*, *67*(1), 168. https://doi.org/10.1186/s40623-015-0334-8

Chaston, C. C., Bonnell, J. W., Clausen, L., & Angelopoulos, V. (2012). Correction to energy transport by kinetic-scale electromagnetic waves in fast plasma sheet flows. *Journal of Geophysical Research*, *117*, A09202. https://doi.org/10.1029/2012JA018476

Chi, P. J., Russell, C. T., & Ohtani, S. (2009). Substorm onset timing via traveltime magnetoseismology. *Geophysical Research Letters*, *36*, L08107. https://doi.org/10.1029/2008GL036574

Davis, T. N. (1962). The morphology of the auroral displays of 1957-1958: 1. Statistical analyses of Alaska data. *Journal of Geophysical Research*, *67*(1), 59–74. https://doi.org/10.1029/JZ067i001p00059

Davis, T. N., & Sugiura, M. (1966). Auroral electrojet activity index AE and its universal time variations. *Journal of Geophysical Research*, *71*(3), 785–801. https://doi.org/10.1029/JZ071i003p00785

Donovan, E., Liu, W., Liang, J., Spanswick, E., Voronkov, I., Connors, M., & Rae, I. J. (2008). Simultaneous THEMIS in situ and auroral observations of a small substorm. *Geophysical Research Letters*, *35*, L17S18. https://doi.org/10.1029/2008GL033794

Elphinstone, R. D., Hearn, D. J., Cogger, L. L., Murphree, J. S., Singer, H., Sergeev, V., & Feldstein, Y. I. (1995). Observations in the vicinity of substorm onset: Implications for the substorm process. *Journal of Geophysical Research*, *100*(A5), 7937. https://doi.org/10.1029/94JA02938

Ergun, R. E., Goodrich, K. A., Stawarz, J. E., Andersson, L., & Angelopoulos, V. (2015). Large-amplitude electric fields associated with bursty bulk flow braking in the Earth's plasma sheet. *Journal of Geophysical Research: Space Physics*, *120*, 1832–1844. https://doi.org/10.1002/2014JA020165

Ferdousi, B., & Raeder, J. (2016). Signal propagation time from the magnetotail to the ionosphere: OpenGGCM simulation. *Journal of Geophysical Research: Space Physics*, *121*, 6549–6561. https://doi.org/10.1002/2016JA022445

Forsyth, C., Rae, I. J., Coxon, J. C., Freeman, M. P., Jackman, C. M., Gjerloev, J., & Fazakerley, A. N. (2015). A new technique for determining Substorm Onsets and Phases from Indices of the Electrojet (SOPHIE). *Journal of Geophysical Research: Space Physics*, *120*, 10,592–10,606. https://doi.org/10.1002/2015JA021343

Frey, H. U., & Mende, S. B. (2006). Substorm onsets as observed by IMAGE-FUV (Tech. Rep.). https://www.ics8.ca/proc_files/frey.pdf

Frey, H. U., Mende, S. B., Angelopoulos, V., & Donovan, E. F. (2004). Substorm onset observations by IMAGE-FUV. *Journal of Geophysical Research*, *109*, A10304. https://doi.org/10.1029/2004JA010607

Friedrich, E., Samson, J. C., & Voronkov, I. (2001). Ground-based observations and plasma instabilities in auroral substorms. *Physics of Plasmas*, *8*(4), 1104. https://doi.org/10.1063/1.1355678

Gjerloev, J. W. (2009). A global ground-based magnetometer initiative. *Eos, Transactions American Geophysical Union*, *90*(27), 230. https://doi.org/10.1029/2009EO270002

Gjerloev, J. W. (2012). The SuperMAG data processing technique. *Journal of Geophysical Research*, *117*, A09213. https://doi.org/10.1029/2012JA017683

Henderson, M. G. (1994). Implications of Viking imager results for substorm models (Thesis PH.D.), UNIVERSITY OF CALGARY (CANADA), 1994.Source: Dissertation Abstracts International, Volume: 56-01, Section: B, page: 0289. https://adsabs.harvard.edu/abs/1994PhDT.....53H

Henderson, M. G. (2009). Observational evidence for an inside-out substorm onset scenario. *Annales Geophysicae*, *27*(5), 2129–2140. https://doi.org/10.5194/angeo-27-2129-2009

Heppner, J. P. (1954). A study of relationships between the Aurora Borealis and the geomagnetic disturbances caused by electric currents in the ionosphere. https://thesis.library.caltech.edu/5004/1/Heppner_jp_1954.pdf

Hones, E. W. (1976). The magnetotail—Its generation and dissipation. *Physics of Solar Planetary Environments*, *2*, 558–571.

Hwang, K. J., Goldstein, M. L., Moore, T. E., Walsh, B. M., Baishev, D. G., Moiseyev, A. V., & Yumoto, K. (2014). A tailward moving current sheet normal magnetic field front followed by an earthward moving dipolarization front. *Journal of Geophysical Research: Space Physics*, *119*, 5316–5327. https://doi.org/10.1002/2013JA019657

Imber, S. M., Slavin, J. A., Auster, H. U., & Angelopoulos, V. (2011). A THEMIS survey of flux ropes and traveling compression regions: Location of the near-Earth reconnection site during solar minimum. *Journal of Geophysical Research*, *116*, A02201. https://doi.org/10.1029/2010JA016026

Jacobs, J. A., Kato, Y., Matsushita, S., & Troitskaya, V. A. (1964). Classification of geomagnetic micropulsations. *Geophysical Journal of the Royal Astronomical Society*, *8*(3), 341–342. https://doi.org/10.1111/j.1365-246X.1964.tb06301.x

Kalmoni, N. M. E., Rae, I. J., Murphy, K. R., Forsyth, C., Watt, C. E., & Owen, C. J. (2017). Statistical azimuthal structuring of the substorm onset arc: Implications for the onset mechanism. *Geophysical Research Letters*, *44*, 2078–2087. https://doi.org/10.1002/2016GL071826

Kalmoni, N. M. E., Rae, I. J., Watt, C. E. J., Murphy, K. R., Forsyth, C., & Owen, C. J. (2015). Statistical characterization of the growth and spatial scales of the substorm onset arc. *Journal of Geophysical Research: Space Physics*, *120*, 8503–8516. https://doi.org/10.1002/2015JA021470

Kalmoni, N. M. E., Rae, I. J., Watt, C. E. J., Murphy, K. R., Samara, M., Michell, R. G., & Forsyth, C. (2018). A diagnosis of the plasma waves responsible for the explosive energy release of substorm onset. *Nature Communications*, *9*(1), 4806. https://doi.org/10.1038/s41467-018-07086-0

Kataoka, R., Miyoshi, Y., Sakanoi, T., Yaegashi, A., Shiokawa, K., & Ebihara, Y. (2011). Turbulent microstructures and formation of folds in auroral breakup arc. *Journal of Geophysical Research*, *116*, A00K02. https://doi.org/10.1029/2010JA016334

Keiling, A. (2012). Pi2 pulsations driven by ballooning instability. *Journal of Geophysical Research*, *117*, A03228. https://doi.org/10.1029/2011JA017223

Kepko, L., & Kivelson, M. (1999). Generation of Pi2 pulsations by bursty bulk flows. *Journal of Geophysical Research*, *104*(A11), 25,021–25,034. https://doi.org/10.1029/1999JA900361

Kepko, L., Spanswick, E., Angelopoulos, V., Donovan, E., McFadden, J., Glassmeier, K. H., & Singer, H. J. (2009). Equatorward moving auroral signatures of a flow burst observed prior to auroral onset. *Geophysical Research Letters*, *36*, L24104. https://doi.org/10.1029/2009GL041476

Kistler, L. M., Möbius, E., Baumjohann, W., Paschmann, G., & Hamilton, D. C. (1992). Pressure changes in the plasma sheet during substorm injections. *Journal of Geophysical Research*, *97*(A3), 2973–2983. https://doi.org/10.1029/91JA02802

Lester, M., Hughes, J. W., & Singer, H. J. (1983). Polarization patterns of Pi2 magnetic pulsations and the substorm current wedge. *Journal of Geophysical Research*, *88*(A10), 7958. https://doi.org/10.1029/JA088iA10p07958

Liang, J., Donovan, E. F., Liu, W. W., Jackel, B., Syrjäsuo, M., Mende, S. B., & Connors, M. (2008). Intensification of preexisting auroral arc at substorm expansion phase onset: Wave-like disruption during the first tens of seconds. *Geophysical Research Letters*, *35*, L17S19. https://doi.org/10.1029/2008GL033666

Lui, A. T. Y., Chang, C. L., Mankofsky, A., Wong, H. K., & Winske, D. (1991). A cross-field current instability for substorm expansions. *Journal of Geophysical Research*, *96*(A7), 11,389. https://doi.org/10.1029/91JA00892

Lui, A. T. Y., Volwerk, M., Dunlop, M. W., Alexeev, I. V., Fazakerley, A. N., Walsh, A. P., & Rème, H. (2008). Near-Earth substorm features from multiple satellite observations. *Journal of Geophysical Research*, *113*, A07S26. https://doi.org/10.1029/2007JA012738

Mann, I. R., Milling, D. K., Rae, I. J., Ozeke, L. G., Kale, A., Kale, Z. C., & Singer, H. J. (2008). The upgraded CARISMA magnetometer array in THEMIS era. *Space Science Reviews*, *141*(1-4), 413–451. https://doi.org/10.1007/s11214-008-9457-6

McFadden, J. P., Carlson, C. W., Larson, D., Ludlam, M., Abiad, R., Elliott, B., & Angelopoulos, V. (2009). The THEMIS ESA plasma instrument and in-flight calibration, *The THEMIS Mission* (pp. 277–302). New York, NY: Springer New York. https://doi.org/10.1007/978-0-387-89820-9_13

McPherron, R. L. (1970). Growth phase of magnetospheric substorms (Vol. 75; Tech. Rep. No. 28). https://citeseerx.ist.psu.edu/viewdoc/download?doi=10.1.1.452.9720&rep=rep1&type=pdf

McPherron, R. L., Aubry, M. P., Russell, C. T., & Coleman, P. J. (1973). Satellite studies of magnetospheric substorms on August 15, 1968 4. Ogo 5 magnetic field observations. *Journal of Geophysical Research*, *78*(16), 3068–3078. https://www.researchgate.net/profile/Robert_Mcpherron/publication/254933902_Satellite_Studies_of_Magnetospheric_Substorms_on_August_15_1968/links/5adf4d5aa6fdcc29358e13ed/Satellite-Studies-of-Magnetospheric-Substorms-on-August-15-1968.pdf

Mende, S. B., Carlson, C. W., Frey, H. U., Peticolas, L. M., & Østgaard, N. (2003). FAST and IMAGE-FUV observations of a substorm onset. *Journal of Geophysical Research*, *108*(A9), 1344. https://doi.org/10.1029/2002JA009787

Mende, S. B., Harris, S. E., Frey, H. U., Angelopoulos, V., Russell, C. T., Donovan, E., & Peticolas, L. M. (2008). The THEMIS array of ground-based observatories for the study of auroral substorms. *Space Science Reviews*, *141*(1-4), 357–387. https://doi.org/10.1007/s11214-008-9380-x

Milling, D. K., Rae, I. J., Mann, I. R., Murphy, K. R., Kale, A., Russell, C. T., & Mende, S. (2008). Ionospheric localisation and expansion of long-period Pi1 pulsations at substorm onset. *Geophysical Research Letters*, *35*, L17S20. https://doi.org/10.1029/2008GL033672

Motoba, T., Hosokawa, K., Kadokura, A., & Sato, N. (2012). Magnetic conjugacy of northern and southern auroral beads. *Geophysical Research Letters*, *39*, L08108. https://doi.org/10.1029/2012GL051599

Motoba, T., Ohtani, S., Donovan, E. F., & Angelopoulos, V. (2015). On a possible connection between the longitudinally propagating near-Earth plasma sheet and auroral arc waves: A reexamination. *Journal of Geophysical Research: Space Physics*, *120*, 432–444. https://doi.org/10.1002/2014JA020694

Murphy, K. R., Jonathan Rae, I., Mann, I. R., Milling, D. K., Watt, C. E., Ozeke, L., & Russell, C. T. (2009). Wavelet-based ULF wave diagnosis of substorm expansion phase onset. *Journal of Geophysical Research*, *114*, A00C16. https://doi.org/10.1029/2008JA013548

Murphy, K. R., Mann, I. R., Rae, I. J., Walsh, A. P., & Frey, H. U. (2014). Inner magnetospheric onset preceding reconnection and tail dynamics during substorms: Can substorms initiate in two different regions? *Journal of Geophysical Research: Space Physics*, *119*, 9684–9701. https://doi.org/10.1002/2014JA019795

Murphy, K. R., Rae, I. J., Mann, I. R., & Milling, D. K. (2011). On the nature of ULF wave power during nightside auroral activations and substorms: 1. Spatial distribution. *Journal of Geophysical Research*, *116*, A00I21. https://doi.org/10.1029/2010JA015757

Murphy, K. R., Rae, I. J., Mann, I. R., Walsh, A. P., Milling, D. K., & Kale, A. (2011). The dependence of Pi2 waveforms on periodic velocity enhancements within bursty bulk flows. *Annales Geophysicae*, *29*(3), 493–509. https://doi.org/10.5194/angeo-29-493-2011

Nagai, T., Mukai, T., Yamamoto, T., Nishida, A., Kokubun, S., & Lepping, R. P. (1997). Plasma sheet pressure changes during the substorm growth phase. *Geophysical Research Letters*, *24*(8), 963–966. https://doi.org/10.1029/97GL00374

Nagai, T., Shinohara, I., Zenitani, S., Nakamura, R., Nakamura, T. K. M., Fujimoto, M., & Mukai, T. (2013). Three-dimensional structure of magnetic reconnection in the magnetotail from geotail observations. *Journal of Geophysical Research: Space Physics*, *118*, 1667–1678. https://doi.org/10.1002/jgra.50247

Nishimura, Y., Lyons, L., Zou, S., Angelopoulos, V., & Mende, S. (2010). Substorm triggering by new plasma intrusion: THEMIS all-sky imager observations. *Journal of Geophysical Research*, *115*, A07222. https://doi.org/10.1029/2009JA015166

Nishimura, Y., Yang, J., Pritchett, P. L., Coroniti, F. V., Donovan, E. F., Lyons, L. R., & Mende, S. B. (2016). Statistical properties of substorm auroral onset beads/rays. *Journal of Geophysical Research: Space Physics*, *121*, 8661–8676. https://doi.org/10.1002/2016JA022801

Olson, J. V. (1999). Pi2 pulsations and substorm onsets: A review. *Journal of Geophysical Research*, *104*(A8), 17,499–17,520. https://doi.org/10.1029/1999JA900086

Panov, E. V., Sergeev, V. A., Pritchett, P. L., Coroniti, F. V., Nakamura, R., Baumjohann, W., & McFadden, J. P. (2012). Observations of kinetic ballooning/interchange instability signatures in the magnetotail. *Geophysical Research Letters*, *39*, L08110. https://doi.org/10.1029/2012GL051668

Rae, I. J., Mann, I. R., Angelopoulos, V., Murphy, K. R., Milling, D. K., Kale, A., & Donovan, E. F. (2009). Near-Earth initiation of a terrestrial substorm. *Journal of Geophysical Research*, *114*, A07220. https://doi.org/10.1029/2008JA013771

Rae, I. J., Mann, J. R., Murphy, I. R., Milling, K. R., Parent, D. K., Angelopoulos, A., & Russell, S. B. (2009). Timing and localization of ionospheric signatures associated with substorm expansion phase onset. *Journal of Geophysical Research*, *114*, A00C09. https://doi.org/10.1029/2008JA013559

Rae, I. J., Murphy, K. R., Watt, C. E. J., & Mann, I. R. (2011). On the nature of ULF wave power during nightside auroral activations and substorms: 2. Temporal evolution. *Journal of Geophysical Research*, *116*, A00I22. https://doi.org/10.1029/2010JA015762

Rae, I. J., Murphy, K. R., Watt, C. E. J., Mann, I. R., Yao, Z., Kalmoni, N. M. E., & Milling, D. K. (2017). Using ultra-low frequency waves and their characteristics to diagnose key physics of substorm onset. *Geoscience Letters*, *4*(1), 23. https://doi.org/10.1186/s40562-017-0089-0

Rae, I. J., & Watt, C. E. (2016). ULF waves above the nightside auroral oval during substorm onset, *Low-Frequency Waves in Space Plasmas* (pp. 99–120). Washington, DC: American Geophysical Union (AGU). https://doi.org/10.1002/9781119055006.ch7

Rae, I. J., Watt, C. E. J., Mann, I. R., Murphy, K. R., Samson, J. C., Kabin, K., & Angelopoulos, V. (2010). Optical characterization of the growth and spatial structure of a substorm onset arc. *Journal of Geophysical Research*, *115*, A10222. https://doi.org/10.1029/2010JA015376

Rae, I. J., Watt, C. E. J., Murphy, K. R., Frey, H. U., Ozeke, L. G., Milling, D. K., & Mann, I. R. (2012). The correlation of ULF waves and auroral intensity before, during and after substorm expansion phase onset. *Journal of Geophysical Research*, *117*, A08213. https://doi.org/10.1029/2012JA017534

Rong, Z. J., Wan, W. X., Shen, C., Li, X., Dunlop, M. W., Petrukovich, A. A., & Lucek, E. (2011). Statistical survey on the magnetic structure in magnetotail current sheets. *Journal of Geophysical Research*, *116*, A09218. https://doi.org/10.1029/2011JA016489

Roux, A., Perraut, S., Robert, P., Morane, A., Pedersen, A., Korth, A., & Pellinen, R. (1991). Plasma sheet instability related to the westward traveling surge. *Journal of Geophysical Research*, *96*(A10), 17,697. https://doi.org/10.1029/91JA01106

Runov, A., Sergeev, V. A., Baumjohann, W., Nakamura, R., Apatenkov, S., Asano, Y., & Klecker, B. (2005). Electric current and magnetic field geometry in flapping magnetotail current sheets. *Annales Geophysicae*, *23*(4), 1391–1403. https://hal.archives-ouvertes.fr/hal-00329405

Russell, C. T., Chi, P. J., Dearborn, D. J., Ge, Y. S., Kuo-Tiong, B., Means, J. D., & Snare, R. C. (2008). THEMIS ground-based magnetometers. *Space Science Reviews*, *141*(1-4), 389–412. https://doi.org/10.1007/s11214-008-9337-0

Saito, T. (1969). Geomagnetic pulsations. *Space Science Reviews*, *10*(3), 319–412. https://doi.org/10.1007/BF00203620

Saito, M. H., Miyashita, Y., Fujimoto, M., Shinohara, I., Saito, Y., & Mukai, T. (2008). Modes and characteristics of low frequency MHD waves in the near Earth magnetotail prior to dipolarization: Fitting method. *Journal of Geophysical Research*, *113*, A06201. https://doi.org/10.1029/2007JA012778

Sakaguchi, K., Shiokawa, K., Ieda, A., Nomura, R., Nakajima, A., Greffen, M., & Lessard, M. (2009). Fine structures and dynamics in auroral initial brightening at substorm onsets. *Annales Geophysicae*, *27*(2), 623–630. https://doi.org/10.5194/angeo-27-623-2009

Samson, J. C., Rankin, R., & Tikhonchuk, V. T. (2003). Optical signatures of auroral arcs produced by field line resonances: Comparison with satellite observations and modeling. *Annales Geophysicae*, *21*(4), 933–945. https://hal.archives-ouvertes.fr/hal-00329249

Shiokawa, K., Baumjohann, W., & Haerendel, G. (1997). Braking of high-speed flows in the near-Earth tail. *Geophysical Research Letters*, *24*(10), 1179–1182. https://doi.org/10.1029/97GL01062

Slavin, J. A., Smith, E. J., Sibeck, D. G., Baker, D. N., Zwickl, R. D., & Akasofu, S. I. (1985). An ISEE 3 study of average and substorm conditions in the distant magnetotail. *Journal of Geophysical Research*, *90*(A11), 10,875. https://doi.org/10.1029/JA090iA11p10875

Slavin, J. A., Tanskanen, E. I., Hesse, M., Owen, C. J., Dunlop, M. W., Imber, S., & Glassmeier, K. H. (2005). Cluster observations of traveling compression regions in the near-tail. *Journal of Geophysical Research*, *110*, A06207. https://doi.org/10.1029/2004JA010878

Sun, W. J., Fu, S. Y., Wei, Y., Yao, Z. H., Rong, Z. J., Zhou, X. Z., & Shen, X. C. (2017). Plasma sheet pressure variations in the near-Earth magnetotail during substorm growth phase: THEMIS observations. *Journal of Geophysical Research: Space Physics*, *122*, 12,212–12,228. https://doi.org/10.1002/2017JA024603

Tsyganenko, N. A., & Sitnov, M. I. (2005). Modeling the dynamics of the inner magnetosphere during strong geomagnetic storms. *Journal of Geophysical Research*, *110*, A03208. https://doi.org/10.1029/2004JA010798

Uritsky, V. M., Liang, J., Donovan, E., Spanswick, E., Knudsen, D., Liu, W., & Glassmeier, K. H. (2009). Longitudinally propagating arc wave in the pre-onset optical aurora. *Geophysical Research Letters*, *36*, L21103. https://doi.org/10.1029/2009GL040777

Viñas, A. F., & Madden, T. R. (1986). Shear flow-ballooning instability as a possible mechanism for hydromagnetic fluctuations. *Journal of Geophysical Research*, *91*(A2), 1519. https://doi.org/10.1029/JA091iA02p01519

Voronkov, I., Donovan, E. F., & Samson, J. C. (2003). Observations of the phases of the substorm. *Journal of Geophysical Research*, *108*(A2), 1073. https://doi.org/10.1029/2002JA009314

Voronkov, I., Rankin, R., Frycz, P., Tikhonchuk, V. T., & Samson, J. C. (1997). Coupling of shear flow and pressure gradient instabilities. *Journal of Geophysical Research*, *102*(A5), 9639–9650. https://doi.org/10.1029/97JA00386

Walsh, A. P., Haaland, S., Forsyth, C., Keesee, A. M., Kissinger, J., Li, K., & Taylor, M. G. G. T. (2014). Dawn-dusk asymmetries in the coupled solar wind-magnetosphere-ionosphere system: A review. *Annales Geophysicae*, *32*(7), 705–737. https://doi.org/10.5194/angeo-32-705-2014

Walsh, A. P., Owen, C. J., Fazakerley, A. N., Forsyth, C., & Dandouras, I. (2011). Average magnetotail electron and proton pitch angle distributions from Cluster PEACE and CIS observations. *Geophysical Research Letters*, *38*, L06103. https://doi.org/10.1029/2011GL046770

Walsh, A. P., Rae, I. J., Fazakerley, A. N., Murphy, K. R., Mann, I. R., Watt, C. E. J., & Zhang, T. L. (2010). Comprehensive ground-based and in situ observations of substorm expansion phase onset. *Journal of Geophysical Research*, *115*, A00I13. https://doi.org/10.1029/2010JA015748

Watt, C. E. J., & Rankin, R. (2010). Do magnetospheric shear Alfvén waves generate sufficient electron energy flux to power the aurora? *Journal of Geophysical Research*, *115*, A07224. https://doi.org/10.1029/2009JA015185

Watt, C. E. J., & Rankin, R. (2012). Alfvén wave acceleration of auroral electrons in warm magnetospheric plasma. In A. Keiling, E. Donovan, F. Bagenal, & T. Karlsson (Eds.), *Auroral Phenomenology and Magnetospheric Processes: Earth and Other Planets. Geophysical Monograph (197)* (pp. 251–260). Washington, DC: American Geophysical Union (AGU). https://doi.org/10.1029/2011GM001171

Xing, X., Lyons, L. R., Angelopoulos, V., Larson, D., Carlson, C., Runov, A., & Auster, U. (2010). Plasma sheet pressure evolution related to substorms. *Journal of Geophysical Research*, *115*, A01212. https://doi.org/10.1029/2009JA014315